Vibrational Dynamics, Mode Coupling, and Structural Constraints for Acetylproline-NH_2

Igor V. Rubtsov and Robin M. Hochstrasser*

Department of Chemistry, University of Pennsylvania, Philadelphia, Pennsylvania 19104-6323

Received: March 29, 2002; In Final Form: June 13, 2002

Vibrational relaxation, mode coupling, and peptide structural constraints were obtained by femtosecond two-dimensional vibrational spectroscopy of an acetylproline-NH_2 model dipeptide. Three high-frequency vibrational modes were examined, two amide-I modes (1693 and 1633 cm^{-1}) and the amide-II amino end mode (1580 cm^{-1}). Efficient vibrational energy transfer between amide-I and amide-II bands located on the same amide has been clearly observed ($\tau \sim 3.1$ ps), which accounts for ~36% of all deactivation pathways of the excited amide-I mode. The evolution of the transient spectral shape (cross-peak) as a result of vibrational energy transfer has been observed for the first time. The ET from the amide-I (acetyl end) band to the amide-II (amino end) band was detected (~10 ps). However, no clear energy transfer between two amide-I bands was seen, yielding an upper limit for the rate constant of $(20\ ps)^{-1}$. A switch of the transient signal from a transition of the pumped state to an overtone (diagonal peak) to one involving a combination band (off-diagonal peak) was clearly demonstrated. This process provides an explanation for the nonexponential decay of the transient spectrum of each of the oscillators. A long-lived signal (cross-peak) was detected in each of the amide-I bands when the other amide-I band was excited, indicating the existence of at least one vibration in the molecule which remains excited for much longer than the average lifetime of the three vibrations being studied. The decay time (~10 ps) of this signal represents one signature of the vibrational cooling of the dipeptide by energy transfer to the solvent. The angles between the transition dipoles of these modes given by the polarization measurements were close to those of a C_7 conformation. The magnitudes of the coupling between the three vibrational modes were determined from a transition charge model of the off diagonal anharmonicity. The values obtained for the amide-I/amide-I and the amide-I/amide-II interactions are about twice those calculated from a dipole−dipole interaction potential based on a C_7 conformation.

Introduction

Vibrational energy redistribution in peptides is central to understanding biological mechanisms of vibrational energy transduction and chemical reactions in protein environments. Vibrational dynamics induced by structural fluctuations of surrounding atoms are essential components of the rates, pathways, and efficiencies of reactions in condensed phases. Therefore, a detailed microscopic description of them is needed. The field of vibrational energy relaxation in liquid solutions has been reviewed frequently and from various perspectives.[1−11] Although, as these reviews attest, there exists a global theoretical framework of vibrational energy relaxation in condensed phases; only a few specific experimental results, mainly for diatomic molecules[12−18] or ions,[19−22] have been brought satisfactorily into relationship with theoretical simulations. There is no general predictive theory in place for polyatomic molecules. In particular, the interplay of dynamics induced by forces that might be considered intramolecular (IVR) with those that involve solvent (EVR)[4,23,24] are not yet fully delineated.

The recent experimental developments in two-dimensional infrared spectroscopy of peptides and proteins[25−29,30,31] have made clear the exciting possibilities for such methods in the determination of structures and conformational dynamics of biologically interesting molecules, yet a much more complete characterization of the vibrational dynamics is needed before their full potential can be realized. There are now several examples where vibrational relaxation has been measured in peptides or proteins. The structurally sensitive amide-I mode relaxes in ca. 1 ps in most cases[26] implying that it is strongly coupled to other internal modes (IVR). This relatively fast relaxation restricts the size of the vibrational excitations in proteins and makes it more challenging to measure the amide-I excitation exchange dynamics between different peptide units in a polypeptide chain. This transfer is likely to be dependent on the local structure of the amide unit, so one way to evaluate it is to examine the relaxation properties of small peptides where it is experimentally more straightforward to excite one unit and make observations of the other. Basic principles of quantum relaxation dynamics[32] suggest that the mechanisms of such transfer should originate from fluctuations in the energy gaps and couplings, in this case between the amide units.[33,34] It is therefore necessary to determine experimentally not only the relaxation rates but also the couplings between the peptide units and their distributions. Since there are multiple pathways involved, the processes of interest are complex, the rules governing them are not yet evident, and important questions remain to be answered. For example: What are the main deactivation channels? How does the relaxation time depend on the vibrational mode excited? What range of time scales is spanned by energy transfer between different amide-I modes? Should these vibrations be treated as localized or delocalized? Is the coupling mechanism due to interactions between transition charges or is it mechanical anharmonicity?

To approach these questions, infrared subpicosecond transient absorption experiments on acetylproline-NH_2 (AcP) dipeptide in methylene chloride were performed. Spectrally narrow, tunable, mid-IR light pulses were generated and used to excite amide-I and amide-II vibrations in the peptide. Observations

* To whom correspondence should be addressed.

10.1021/jp020837b CCC: $22.00
Published on Web 08/14/2002

of the time evolution of the transient spectrum permitted measurements of the coupling and energy transfer between the different modes. In addition, using principles outlined previously,[25−27] structural constraints were generated.

Experimental Methods

Mid-IR Transient Absorption Spectrometer. The mid-IR pump/probe transient absorption spectrometer is based on a Ti:S laser system consisting of a fiber oscillator and a regenerative amplifier (Clark-MXR, CPA-2001), which delivers a pulse train of 775-nm light (pulse duration, ~120 fs; repetition rate, 1 kHz; pulse energy, ~750 μJ). A commercial OPA (Clark-MXR), modified to improve stability of the pulse train, provides signal and idler pulses with total energy ~50 μJ/pulse. The difference frequency was generated in a 2-mm $AgGaS_2$ type I crystal, providing the mid-IR beam (bandwidth, 150 cm^{-1} (fwhm); pulse durations, ~200 fs; pulse energy ~0.6 μJ at ~6 μm). Pump, probe, and reference beams were separated by a wedged CaF_2 window. After a variable delay, the pump pulses were filtered by a tunable Fabry−Perot (FP) interferometer in the manner previously reported.[26] The two interferometer IR mirrors had reflectivity ~92%. One of them was mounted on a computer-controlled piezoelectric actuator to control the mirror spacing. The bandwidth of the resulting tunable pump pulses was ~22 cm^{-1}. Pump and probe beams were focused into the sample cell with an f/10 cm, 90° parabolic mirror, yielding a spot size of ~70 μm for the probe and 150 μm for the pump. The polarization of the probe beam was controlled by two wire-grid polarizers. The pump beam was chopped at half the laser repetition rate to eliminate low-frequency fluctuations of the IR intensity. The probe and reference beams, vertically displaced, were focused onto the entrance slit of a monochromator. Two MCT detectors were used to measure the probe and reference beam intensities. A spectral resolution was ~4 cm^{-1}. The anisotropy measurements were accomplished by rotating the polarization of the probe beam.

Sample Preparation. The AcPro-NH_2 dipeptide in methylene chloride (150 mM) was contained in a CaF_2 cuvette, with a 56-μm spacing. All experiments were carried out at ambient temperature (23 ± 1 °C).

Results and Discussion

The FTIR absorption spectrum of the AcP dipeptide in a range from 1540 to 1725 cm^{-1} is shown in Figure 1. It has three absorption bands, an amide-II, amine end band (A:1580 cm^{-1}), two amide-I bands (B: 1633 cm^{-1}, acetyl end; and C: 1693 cm^{-1}, amine end) separated by about 50 cm^{-1}. Each of the three bands were excited by spectrally narrow mid-IR excitation pulses, and transient difference absorption (ΔD) spectra, covering the region from 1520 to 1735 cm^{-1}, were detected at several time delays for each excitation wavelength.

General Description of the Transient Spectrum. The transient signal (see Figure 2) is a sum of a transient absorption ($v = 1 \rightarrow v = 2$), ground-state bleach (0→1), and stimulated emission (1→0). The frequency of the 1→2 transition is anharmonically shifted from the 0→1 transition, and its extinction coefficient is twice as large as that of 0→1 in a harmonic approximation. The anharmonic shift determines the shape of the diagonal transient spectrum, which exhibits an absorption on the low-frequency side of the excited band and bleach on the high-frequency side (diagonal signal) (Figure 2a). The diagonal anharmonicity, Δ_{ii} for mode i, is always found to be close to 13 cm^{-1}. In addition to the diagonal spectral feature, transient signals in the regions of the bands not directly excited

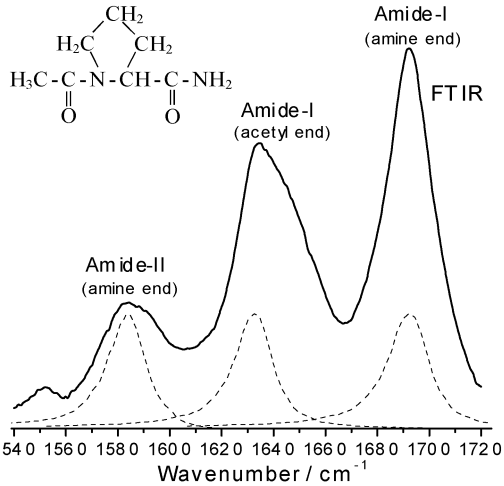

Figure 1. FTIR spectrum of AcPro-NH_2 in methylene chloride. Spectra of the excitation pulses used in the time-resolved experiments are shown by dotted lines.

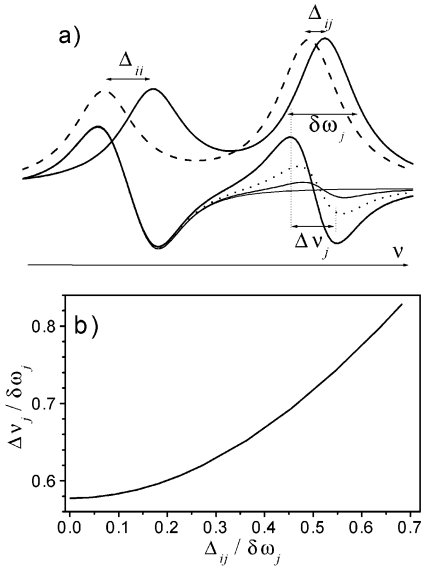

Figure 2. (a) Expected features of the pump−probe spectra for typical values of the diagonal, Δ_{ii}, and off-diagonal, Δ_{ij}, anharmonicity and line width $\delta\omega_i$. The observed shift in the cross-peak region of the difference spectrum is designated as $\Delta\nu_j$. A difference spectrum for a very small coupling is also shown. (b) The peak separation of the transient signal as a function of anharmonicity, both given as ratios to the line width.

were observed. These are the cross-peak signals. The presence of these signals at the instant of excitation indicates that there is an off-diagonal anharmonicity Δ_{ij} caused by the coupling between vibrations. Because of the finite line widths, which can differ for 0−1 and 1−2 transitions, and the effects of hole burning, which are determined by the excitation pulse spectrum and the inhomogeneous distribution, the observed peak separations do not necessarily yield the anharmonicities directly. However, the underlying parameters are readily obtained by fitting. In addition to the detailed fitting of the data, the results of which are given in the Tables and Figures, we have found it useful to describe the observations in terms of a parameter $\eta_{ij} = \Delta D_j \epsilon_i / \Delta D_i \epsilon_j$ where ϵ_i and ϵ_j are the peak extinctions for modes i and j in the linear spectrum. This parameter addresses the relative strengths of cross-peaks which are determined by the off-diagonal anharmonicity. The peak separation between the bleach and absorption parts of the transient signal ($\Delta\nu$) provides another useful qualitative measure of the cross-peak anharmo-

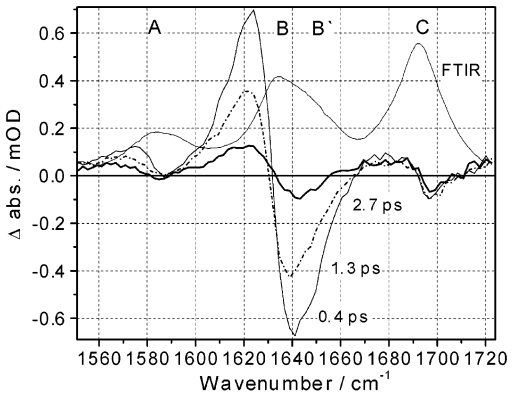

Figure 3. Transient absorption spectra at three delay times (0.4, 1.3, and 2.7 ps) obtained for the B-band excitation (1633 cm^{-1}) at magic angle polarization. The FTIR spectrum is shown by the thin line.

nicity that is also mentioned in the description of the results. Figure 2b shows how values of $\Delta\nu$ are related to anharmonicities. All transient spectra were globally fitted using all the spectral and kinetic information along with the FTIR spectrum. Lorenzian line shapes were assumed for all transitions after it was ascertained that the results were not sensitive to this assumption.

At sufficiently early times, the spectra reflect the interaction of the pumped vibrations with other modes. For example, if the B band is pumped, the signal at the position of the C band will reflect interaction, or mixed mode anharmonicity, of the B and C states. On the other hand, even at 0.4-ps delay some of the initially excited molecules might have relaxed into modes other than A, B, and C. If the population from the B state were to relax to a state, D, which is also coupled to the C state, the signal at the C-band position would reflect the C−D coupling. Therefore, to identify the coupling between the A, B, and C states, which is the object of the present work, the signals must be obtained before relaxation scrambles the information.

Signals Following B-Band Excitation. The transient spectra obtained after excitation of the acetyl end amide-I band (B band) are shown in Figure 3. The diagonal peak separation yields a diagonal anharmonicity value of 13 ± 2 cm^{-1}.

The width of the off-diagonal C and A features at 0.4-ps time delay are about 12 and 13 cm^{-1}, respectively, which are both much smaller than the respective C and A diagonal spectral features ($\sim$19 cm^{-1}). The estimate of the anharmonicities based solely on spectral width (Figure 2b) gives $\Delta_{BA} \sim 5$ cm^{-1} and $\Delta_{BC} < 3$ cm^{-1}. The estimate based on the amplitudes of the signals, $\eta_{BA} = 0.22$ and $\eta_{BC} = 0.088$, gives similar values, $\Delta_{BA} \sim 5.5$ cm^{-1} and $\Delta_{BC} \sim 1.8$ cm^{-1}.

An interesting feature can be seen in the A-band region (Figure 3): at later times, the spectrum broadens and slightly shifts to smaller frequencies. Exactly this kind of behavior is expected if there is a population transfer from state B to state A. The initial coupling signal involves the transition from B to the combination band B + A, which peaks at $\omega_A-\Delta_{AB}$. Relaxation from B→A introduces a transition at $\omega_A-\Delta_{AA}$. The early time anharmonicity ($\Delta_{AB} \sim 5.5$ cm^{-1}) is much smaller than the diagonal anharmonicity, Δ_{AA}, of the A band (13 cm^{-1}), indicating that the early time signal at A-band region is dominated by a BA coupling but not A-band population. The peak separation of the transient spectrum increases from ca. 16.8 cm^{-1} at 1.6-ps delay and ca. 18.2 cm^{-1} at 2.7-ps delay. The latter value is close to the peak separation when the A band is excited directly. A global fit of the complete transient spectra is necessary to obtain the B to A energy-transfer rate constant (see below).

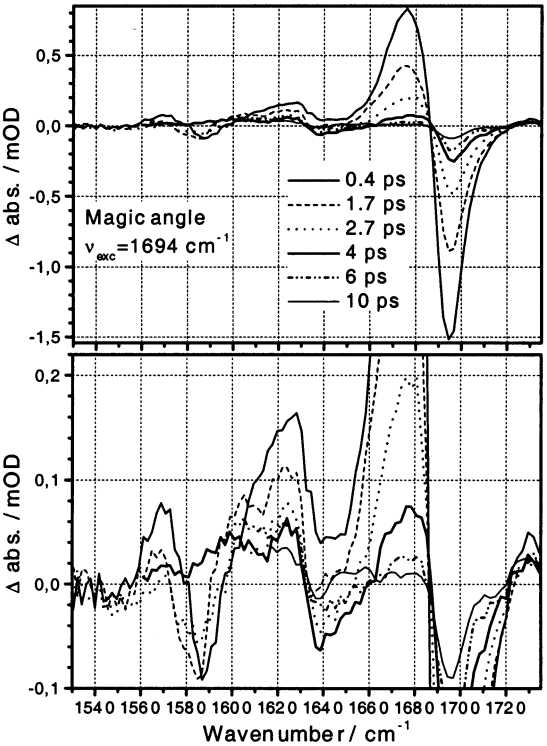

Figure 4. Transient absorption spectra at six delay times (0.4, 1.7, 2.7, 4, 6, and 10 ps) obtained for the C-band excitation (1694 cm^{-1}) at magic angle polarization. The same data on an enlarged scale are shown in the lower panel.

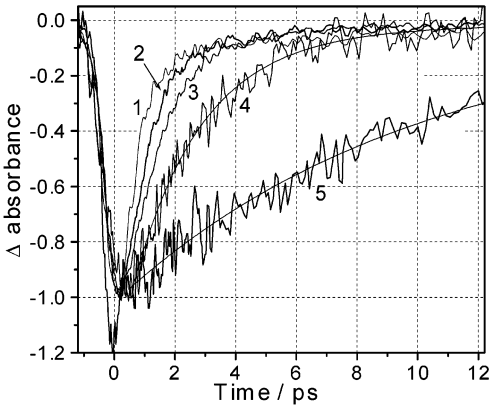

Figure 5. The time dependence of the diagonal A−A (1), B−B (2), and C−C (3) and off-diagonal C−A (4) and B−C (5) bleaching signals. The signals are normalized to the same amplitude at the delay time of 0.4 ps.

The C-band spectral feature on pumping B does not show any broadening with time, indicating that energy transfer from the B to the C state is not efficient. The signal at the C band clearly decays much more slowly than that at the B band (Figure 4). This result suggests that the B population is transferred to modes that are similarly or more strongly coupled to the mode C than is mode B. One of those vibrations is the amide-II vibration (band A). The decay of the transient absorption at 1697 cm^{-1} (Figure 5) involves a time constant of 10 ± 0.5 ps, about 1 order of magnitude larger than the decay time of the population at the B mode which is attributed to the overall cooling of the molecule. Such a manifestation of cooling requires relaxation of the initially excited high-frequency vibrations into low-frequency modes which are weakly coupled to the high-frequency modes. The low-frequency vibrational energy distribution could remain excited for even longer times than those

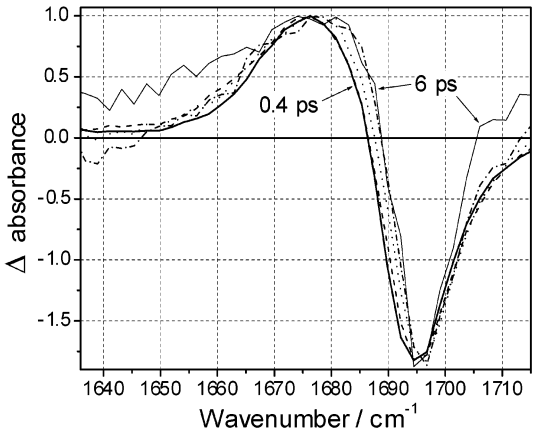

Figure 6. Diagonal transient spectra in the C-band region at different time delays (0.4 ps, thick solid line; 1.7 ps, dashed line; 2.7 ps, dotted line; 4 ps, dashed−dotted line; and 6 ps, thin solid line) normalized to the signal at 0.4 ps. The spectra below 1695 cm^{-1} shift to higher frequency with increasing the delay time, and the bleach spectrum sharpens.

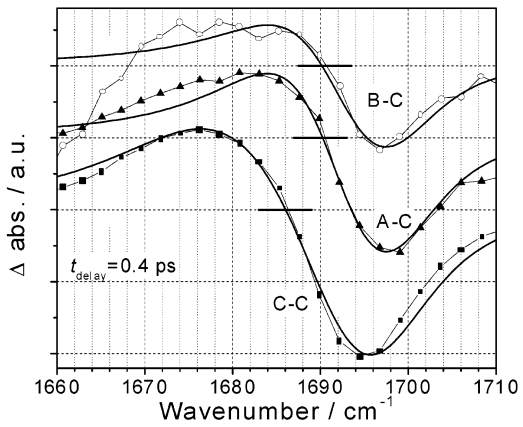

Figure 7. Transient difference spectra in the C-band region obtained at 0.4 ps delay for different excitation wavelengths. The zero lines for each spectrum are shown. The results of the fit are shown by smooth, thick lines (see text).

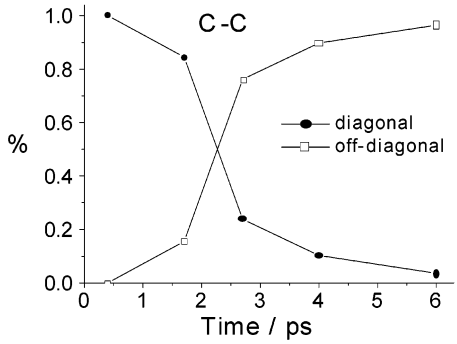

Figure 8. Time dependence of the diagonal and off-diagonal contributions to the C−C transient spectra deduced from the data in Figure 7.

measured if the anharmonic couplings were sufficiently small, although the time of ∼10 ps is not unreasonable for the equilibration time of the solute and solvent [3−5,24,35].

Signals Following C-Band Excitation. A diagonal anharmonicity of $\Delta_{CC} = 13$ cm^{-1} is obtained from the early time transient spectra. The decay of the diagonal signal is nonexponential, but it could be fit by a biexponential function with characteristic times of 1.2 ± 0.1 (93%) and 6 ± 2 (7%) ps.

The ratio of amplitudes of the signal at the B-band and C-band regions yields $\eta_{CB} = 0.085$ which is very close to the value obtained for B-band excitation ($\eta_{BC} = 0.088$). The corresponding off-diagonal anharmonicity is $\Delta_{CB} \leq 2$ cm^{-1}. The peak separation of the signal in the B-band region is about 12.1 cm^{-1}, in agreement with the calculated anharmonicity. The peak separation of the B-region signal does not evolve significantly as would be expected if there were population transfer from the C to the B mode. The amplitude of the signal at the B-band region decays with a characteristic time of 10.6 ± 1.5 ps, similar to the decay of the B−C signal, manifesting the cooling time of the low-frequency vibrations in the molecule as described above.

The peak separation of the signal at the A-band region at 0.4-ps delay time after pumping C is unexpectedly large (17 cm^{-1}), implying an off-diagonal anharmonicity of ca. 13.0 cm^{-1}. The signal amplitude ratio would be large for such a large off-diagonal anharmonicity, but we found $\eta_{CA} = 0.23$, which corresponds to an off-diagonal anharmonicity of only ∼4 cm^{-1} and an expected peak separation of only ∼13 cm^{-1}. This result is interpreted to mean that at 0.4-ps delay there is already a population in the A band, giving a diagonal contribution to the observed signal at A-band region. The peak separation increases slightly by 1.7-ps delay to 17.5 cm^{-1} but decreases to ∼14.5 cm^{-1} by 2.7 ps. The increase is typical for an increased contribution of the "diagonal" signal (population), while the decrease at 2.7 ps can be caused by an increased off-diagonal contribution. The kinetics measured at 1587 cm^{-1} following excitation of C is dominated by a 2.3-ps decay time which is considerably longer than the 0.55- and 1.2-ps decay times of the A and C states.

The diagonal C-band region spectra (C−C) obtained at different delay times exhibit shift to lower frequency and a sharpening with time (Figure 6). We suggest that these changes are caused by the signal evolving from a diagonal to an off-diagonal character. The C−C spectrum at 10-ps delay becomes very similar in shape to the B−C and A−C spectra indicating that they all involve small anharmonicities of an off-diagonal type. The C−C spectra at different delay times were fitted by varying the contributions of two components—a diagonal type and a typical off-diagonal type (Figure 7). Figure 7 also illustrates the typical quality of global fits to the data. The time dependence of the contribution of the off-diagonal signal in Figure 8 shows that at 4-ps delay the signal is predominantly caused by the off-diagonal contribution. This analysis makes very clear that the nonexponential decay of the conventional pump−probe measurement in the diagonal region (i.e., pump 0→1 and probe in the region of 1→2) is caused by the switch from a diagonal to an off-diagonal signal type.

Signals Following A-Band Excitation. The diagonal anharmonicity of the amide-II (A) band (13 cm^{-1}) is similar to those of the C and B bands. A biexponential fit of the diagonal signal decay gives characteristic times of 0.55 ± 0.05 (92%) and 8 ± 3 (8%) ps, indicating that the A band is significantly coupled to other vibrations in the molecule.

The value of $\Delta\nu$ for the transient spectrum at the B-band region at early times is ∼13 cm^{-1} and does not change with time. The amplitude ratio is $\eta_{AB} = 0.25$, which yields the anharmonicity $\Delta_{AB} \sim 4.5$ cm^{-1}. The spectral shift expected for this anharmonicity is ∼13 cm^{-1} in agreement with the direct observation. When pumping A and probing C, we find $\Delta_{AC} = 3.6$ cm^{-1}. The spectral shift expected for this anharmonicity is ∼13.2 cm^{-1}, which is close to that observed experimentally ($\Delta\nu = 13.8$ cm^{-1}). The amplitude of the signal at the C band decays with a time constant of 3.3 ps. There is no significant time dependence of the C-band transient spectral shape following A-band excitation.

TABLE 1: Experimental Decay Times, Anharmonicities (Δ_{XX}), and Couplings (β_{XX}) of Different Vibrational Modes of AcP in Methylene Chloride and Initial Anisotropy of the Cross-Peaks (r^0_{XX}) and the Angles between the Transition Moments (θ_{XX})

X−Y	decay time/ps	Δ_{XY}/cm^{-1}	β_{XY}/cm^{-1}	r^0_{XY}	θ_{XY}
C−C	1.2 ± 0.1(93%), 6 ± 2(7%)	13 ± 2		0.39 ± 0.03	0
C−B	10.6 ± 1.5	1.3 ± 0.4	±9.5 ± 1.5	0.11 ± 0.05	44 ± 5°
C−A	2.3 ± 0.1(96%), 12 ± 5(4%)	4.1 ± 0.6	±32 ± 3	0.03 ± 0.05	52 ± 5°
B−C	10.0 ± 0.3	1.6 ± 0.4	±10.5 ± 1.5	−0.02 ± 0.05	56 ± 5°
B−B	0.86 ± 0.05 (91%), 4.5 ± 1.5 (9%)	13 ± 2		0.38 ± 0.03	0
B−A	2.4 ± 0.4	6.4 ± 1	±18.6 ± 1.5	0.19 ± 0.05	36 ± 5°
A−C	3.3 ± 0.2	3.5 ± 0.5	±29.6 ± 2	−0.10 ± 0.04	66 ± 5°
A−B	0.64 ± 0.05(78%), 5.1 ± 1(22%)	6.5 ± 1	±18.8 ± 1.6	0.21 ± 0.04	34 ± 4°
A−A	0.55 ± 0.05 (92%), 8 ± 3(8%)	13 ± 2		0.36 ± 0.04	0
A−B\	same as A−B	1.2 ± 0.6	±8.1 ± 2.1	0.2 ± 0.08	35 ± 8
C−B\	same as C−B	5 ± 0.2	±19 ± 4	0.35 ± 0.1	16 ± 15

The Relaxation Dynamics. The various time constants measured in the foregoing pump and probe configurations could not be rationalized on the basis of only the three coupled levels A, B, and C exchanging population with each other. A kinetic model in which the rates are all linearly dependent on the populations of the system required the introduction of other states that could exchange energy and equilibrate with the three states being observed in the experiments. These additional, unidentified states are referred to as reservoir states (R). Physically, the reservoir represents other modes of the system that are anharmonically coupled to the excited states A, B, and C and become populated by relaxation to and from them. The results are based on the data of Table 1. Intra-ABC mode energy transfer is most clearly detected for the B−A and C−A cases. The requirement for the intervention of other states is evident from the lack of correspondence between the diagonal kinetic components A−A, B−B, and C−C and the kinetics found when these states are not pumped directly. Furthermore, the kinetics of a given state can depend on which other state was pumped: for example, C−B and A−B are quite different. We have used the 14 measured time constants to generate a minimal model that involves equilibration with one reservoir state R that cools in 10 ps. The diagonal and off-diagonal anharmonicities were used to evaluate the line shape changes resulting from population flow effects superimposed on the signals from coupling of the pumped and observed modes. The importance of the reservoir state is also clear from the A-state properties. Since the decay of the A state is very fast, its persistence after pumping B must be caused by a repopulation of the A state from the reservoir: the amount of the population accumulated in the state A after B-state excitation is substantial (∼8%). A satisfactory fit of the diagonal component in the A band following B-band excitation and the slow component in the A−A decay are the result of equilibration with the R state. The rate constant for energy transfer from C to A is estimated to be about 0.32 ps^{-1}, which is more than 3 times larger than that from B−A energy transfer. The C−A transfer appears to be a significant channel of the C state deactivation (∼36%). For comparison, the B−A energy transfer channel represents only ∼9% of the total B state decay. Specifying only one reservoir state is only an approximation because it is already clear from the data that other states will be required to complete the model. For example, the repopulation of the A state from the reservoir is not needed to fit the data with C-band excitation. The fit results are summarized in Figure 9. The experiment involved 3 sets of initial conditions,

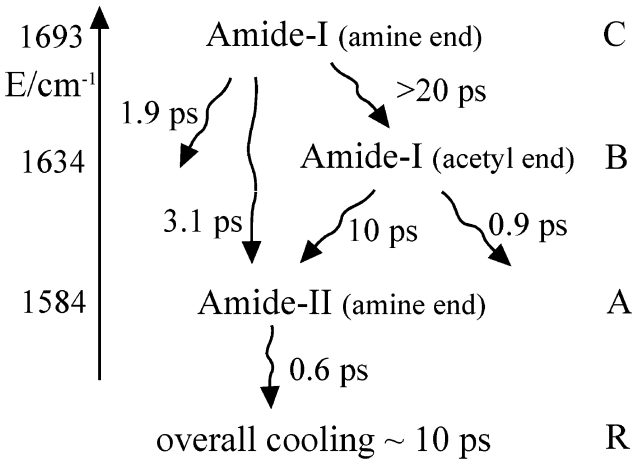

Figure 9. Schematic representation of the main energy-transfer pathways.

6 complete spectra for each initial condition, and continuous kinetic records at 10 frequencies. This overdetermines the 14 required constants. The following rate coefficients were obtained from the fitting: $k_{AB} = 0.08\ ps^{-1}$, $k_{AC} = 0.20\ ps^{-1}$, $k_{AR} = 1.67\ ps^{-1}$; $k_{BA} = 0.10\ ps^{-1}$, $k_{BC} = 0.01\ ps^{-1}$, $k_{BR} = 1.09\ ps^{-1}$; $k_{CA} = 0.32\ ps^{-1}$, $k_{CB} = 0.01\ ps^{-1}$, $k_{CR} = 0.52\ ps^{-1}$; $k_R = 0.12\ ps^{-1}$, $k_{RA} = 0.05\ ps^{-1}$, $k_{RB} < 0.01\ ps^{-1}$, $k_{RC} < 0.01\ ps^{-1}$. The ratio k_{AR}/k_{RA} is ∼30, which, if there was just a single state in the reservoir exchanging population with the A state, would place it at ∼700 cm^{-1} below the A state and imply ∼900 cm^{-1} for its frequency.

The C to A energy-transfer process having the rate constant of 0.32 ps^{-1} is a clear case where we locate an efficient relaxation pathway of the IVR process between the three amide levels. The A and C modes are the amide-I and amide-II modes of the same peptide that involve displacements of similar atoms. Likely, efficient amide-I/amide-II relaxation will be a general property of amides. In contrast, the B-to-A energy-transfer channel, involving transfer between two different sets of atoms, takes 10 ps, showing that amide-I/amide-II relaxation may not be important if the modes are on adjacent units.

Anisotropy of the Coupling Regions and Structural Constraints. The anisotropy of the diagonal peaks were all close to 0.4 as expected from pumping and probing the same transition (Table 1). However, different values were observed for the cross-peaks (see Figure 10 and Tables 1 and 2). Figure 10 illustrates the quality of the global fits to the data. The pump/probe anisotropy is determined by the mean values of the squared cosines of the angles between the transition dipoles of the pumped and probed states:[25,36]

$$r(t) = 0.4\langle P_2[\cos\theta]\rangle R(t) \quad (1)$$

where $R(t)$ is an orientational correlation function and the average is over the distribution of internal angles. At delay times near zero, or in the range when the overall and the internal motion of the molecule can be neglected, the average of $\cos^2\theta$ can be obtained directly from the anisotropy values (Table 2). In the present case, the measured rotational relaxation function decayed on the 8−10 ps time scale. Therefore, the rotational diffusion is negligible during the first 500 fs when the anisotropy measurements were made. The polarization data were obtained for each of the three different excitation wavelengths. The averages $(r_{xy} + r_{yx})/2$ were used to derive the angles for the structural constraints. If the molecule frame transition dipole directions of the amide-I and −II transitions are assumed to be

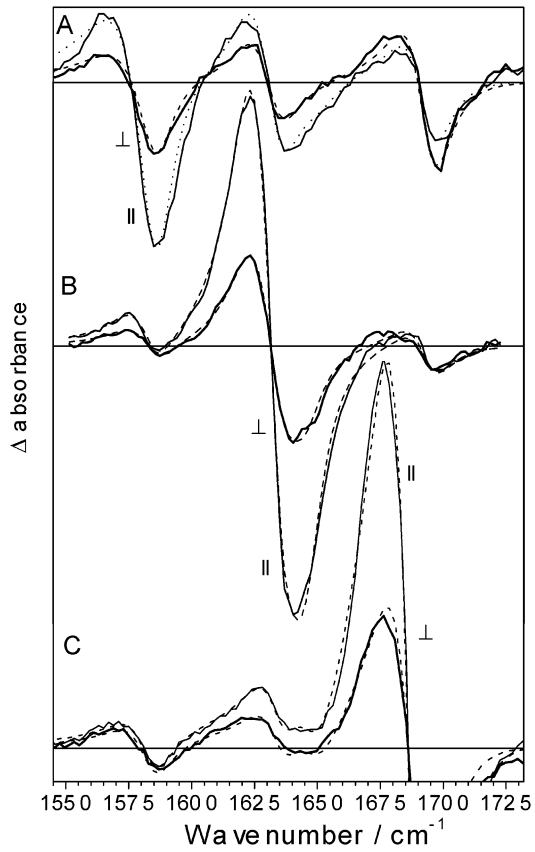

Figure 10. Transient difference spectra for parallel (||, thin solid line) and perpendicular (⊥, thick line) polarizations of the probe light with respect to the pump obtained for (A) 1585 cm^{-1} (A-band) excitation, (B) 1633 cm^{-1} (B-band) excitation, and (C) 1693 cm^{-1} (C-band) excitation at 0.4-ps time delay. The global fit results are given by the dashed lines.

TABLE 2: Angles between Transition Moments (θ_{XY}), Obtained Experimentally and Calculated for a C_7 Conformation

	experimental	C_7 conformation
Am−I(Ac)/Am−I(Am)	$\theta_{CB} = 136 \pm 5°$ $\theta_{BC} = 124 \pm 5°$	$\theta_{BC} = 134 \pm 15°$ [b]
Am−I(Ac)/Am−II	$\theta_{BA} = 36 \pm 5°$ $\theta_{AB} = 34 \pm 3°$	$\theta_{AB} = 35 \pm 15°$ [b]
Am−I(Am)/Am−II	$\theta_{CA} = 128 \pm 5°$ $\theta_{AC} = 114 \pm 5°$	$\theta_{AC} = 144$ °[a]

[a] The direction of the Am−II dipole is assumed to be along C−NH_2 bond. [b] These ranges are estimated from an AM1 semiempirical computation of distributions of C_7 conformations.

transferable from earlier work on other molecules, we can find structures that are consistent with these constraints. The measured angles are consistent with a C_7 internally H-bonded structure dominating the signals (Figure 11 and Table 2). The difference between r_{CA} and r_{AC} is outside of the experimental uncertainty (see Table 2 and Figure 10), and we have no solid explanation for it. One possibility is that a population of another conformation, known to be present from IR COSY studies in $CHCl_3$,[27−29] is excited to different extents in the two experiments. Since this cross-peak anisotropy is close to zero, a small contribution from a different structure could modify the anisotropy significantly. The dihedral angles which correspond to the experimentally determined structure ($\varphi \sim -87°$ and $\psi \sim 65°$) are close to the angles reported for the AcProNHMe (−80, 80).[37]

Interpretation of the Coupling. The experiment measures the diagonal and off-diagonal anharmonicities which determine

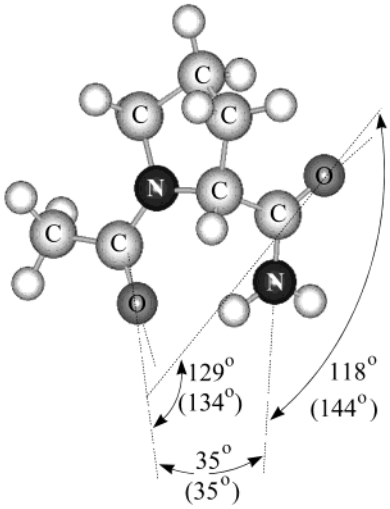

Figure 11. The C_7 structure of AcP. The experimentally determined angles are shown along with the angles (in brackets) determined for the C_7 conformation (see text).

the expansion coefficients of the potential energy in terms of the normal modes. If the coupling between the amide modes were to be reasonably modeled as an excitation exchange, induced by the interaction of the relevant transition charges,[26,38,39] then relationships between the expansion coefficients and these couplings would be established by the experiments. In the weak coupling limit, where the vibrational excitations are approximately localized on the three different modes, the six eigenvalues in the spectral region of two vibrational quanta would be obtained in a straightforward way using perturbation theory. Each combination state is coupled to two overtone states in the harmonic approximation for the matrix elements. The off-diagonal anharmonicity can then be written in terms of the vibrational frequencies ω_i (i = A, B, or C), excitation exchange coupling matrix elements β_{ij}, and the diagonal anharmonicity of modes i and j as

$$\Delta_{ij} = 2\beta^2_{ij}(\Delta_{ii} + \Delta_{jj})/((\omega_i - \omega_j + \Delta_{ii})(\omega_i - \omega_j - \Delta_{ij})) \quad (2)$$

The experiment directly yields all the frequency separations in this formula so values for the coupling matrix elements, β_{ij}, are obtained from the data. These values of β_{ij} required to satisfy Equation 2 are given in Table 1. Although one can obtain the transition-charge interactions from the computed charge fluxes associated with each normal mode,[40] it is useful to test the validity of a dipole−dipole interaction potential for interaction of the transition charges. The matrix elements of the dipole−dipole approximation can be computed from knowledge of the absorption cross sections, the angles obtained from the anisotropy of the cross-peaks, and the distances inferred from conventional chemical connectivity constraints on the basis of these angles. For the AcP amide-I mode at the acetyl end, we find the absorption cross section to be 2.4×10^{-18} cm^2. This yields a transition dipole moment of 0.33 D. Using locations of the point dipoles as defined previously,[26,39] we compute the dipole−dipole coupling as 4.0 and 7.6 cm^{-1} for the B−C and A−B interactions, respectively, using the angular properties of a C_7 structure obtained from the anisotropy measurements. These couplings and the measured interactions of $+10 \pm 2.7$ cm^{-1} and 18.8 ± 2.8 cm^{-1}, respectively, obtained by averaging the values in Table 1 are not in agreement. The results suggest that contribution of the mechanical coupling to the off-diagonal anharmonicity of these modes is significant and that the

transition-charge parts of the excitation-exchange interaction, as computed from the procedure outlined, represent only about half of the coupling. The amide-I and -II transitions (C and A) that are both at the amine end of the peptide are coupled by 29.6−32 cm^{-1} according to Equation 2, but in this case, a transition-charge interaction is not expected to be reasonable because the two modes are in the same spatial region involving the same set of atoms.

An additional structure is clearly present in solution, which can be seen from a splitting of the B band (B and B′ bands and the data in Figure 10). Using the experimentally obtained angles $\theta_{CB'}$ and $\theta_{AB'}$, this minority component is determined to be close to an α-helix type with $\phi \sim -95°$ and $\psi \sim -70°$, which results in the calculated angles between transition moments of $\theta_{CB'} = 17°$ and $\theta_{AB'} \sim 28°$: the experimental angles are 16° and 35°, respectively. In $CHCl_3$[27] the $\theta_{CB'}$ angle is 10°. The transition dipole interaction couplings computed for this structure, $V_{CB'} = 10.6$ cm^{-1} and $V_{AB'} = 3.3$ cm^{-1}, are again about one half the experimentally measured values of 19 ± 4 and 8.1 ± 2.1 cm^{-1}, respectively. Although the pump-probe method of 2D-IR used here provides very precise anisotropy data the effects of the underlying conformational distribution are more clearly separated using IR COSY[27].

Conclusions

Transient infrared spectra of AcPro-NH_2 dipeptide in the amide-I and -II regions were acquired following selective IR excitation of each of the three bands with a spectrally tailored pulse. The anharmonic couplings of the three vibrational modes and mutual orientation of their transition dipoles were determined. The dominant structure was found from anisotropy measurements to be close to the C_7 self-hydrogen-bonded conformation. Mode specific vibrational energy-transfer rates were determined for these modes. Fast energy transfer was observed between the amide-I and amide-II vibrations located on the same amide ($\tau \sim 3.1$ ps) at the amino end of the peptide. This energy transfer is efficient, being responsible for ∼36% of all deactivation channels of the amide-I state. The energy transfer between two amide-I modes is slow with the time constant estimated to be larger than 20 ps. The energy transfer from the acetyl end amide-I mode to the amino end amide-II mode was also observed ($\tau \sim 10$ ps). A simple transition dipole coupling is shown to be completely inadequate to explain the observed off-diagonal anharmonicities. Instead, strong mechanical mode coupling through the mediation of the proline link is invoked.

The shapes of the cross-peak signals change with time. At early time delays and before vibrational energy transfer takes place, the cross-peaks are shaped by the off-diagonal anharmonicities linking each of the pumped and probed modes. Vibrational energy transfer to other modes results in contributions to the cross-peaks from diagonal anharmonicities. The diagonal peaks show the opposite trend: the transient spectrum changes from being determined by the diagonal anharmonicity to one that is caused by intermode coupling. The latter effect largely determines the nonexponential dynamics of the diagonal transient signals.

Long-lived off-diagonal cross-peaks can be seen in both amide-I bands when the other amide-I band is excited. The existence of this slow component implies that there is another mode, or modes, involved in determining the kinetics. These modes, constituting the reservoir, are located lower in frequency than the amide-II (1580 cm^{-1}) band and exhibit long lifetimes. The decay time of ∼10 ps is assigned to the vibrational cooling of the peptide, corresponding to energy transfer to the solvent from the reservoir states. When one state is used to approximate the effect of the reservoir, it is estimated to have a frequency of about 1000 cm^{-1}.

Acknowledgment. This research was supported by grants from NIH and NSF and by instrumentation developed in the NIH Resource RR001348. We are indebted to Professor M. Therien for contributing technical support for this work.

References and Notes

(1) Oxtoby, D. W. *Adv. Chem. Phys.* **1979**, *40*, 1.
(2) Oxtoby, D. W. *Annu. Rev. Phys. Chem.* **1981**, *32*, 77.
(3) Oxtoby, D. W. *Adv. Chem. Phys.* **1981**, *47*, 487.
(4) Owrutsky, J.; Raftery, D.; Hochstrasser, R. M. *Annu. Rev. Phys. Chem.* **1994**, *45*, 519.
(5) Laubereau, A.; Kaiser, W. *Rev. Mod. Phys.* **1978**, *50*, 607.
(6) Laubereau, A.; Fischer, S. F.; Spanner, K.; Kaiser, W. *Chem. Phys.* **1978**, *31*, 335.
(7) Seilmeier, A.; Kaiser, W. In *Ultrashort Laser Pulases*, 2nd ed.; Kaiser, W., Ed.; Springer-Verlag: New York, 1993; p 279.
(8) Heilweil, E. J.; Casassa, M. P.; Cavanagh, R. R.; Stephenson, J. C. *Annu. Rev. Phys. Chem.* **1989**, *40*, 143.
(9) Elsaesser, T.; Kaiser, W. *Annu. Rev. Phys. Chem.* **1991**, *42*, 83.
(10) Anfinrud, P. A.; Johnson, C. K.; Sension, R.; Hochstrasser, R. M. *Ultrafast spectroscopic methods*; VCH Publishers: New York, 1992.
(11) Raftery, D.; Sension, R. J.; Hochstrasser, R. M. In *Activated Barrier Crossing*; Fleming, G. R., Hanggi, P., Eds.; World Scientific Publishing Co. Ltd.: River Edge, NJ, 1993; p 163.
(12) Whitnell, R. M.; Wilson, K. R.; Hynes, J. T. *J. Chem. Phys.* **1992**, *96*, 5354.
(13) Whitnell, R. M.; Wilson, K. R.; Hynes, J. T. *J. Phys. Chem.* **1990**, *94*, 8625.
(14) Gnanakaran, S.; Hochstrasser, R. M. *J. Chem. Phys.* **1996**, *105*, 3486.
(15) Pugliano, N.; Szarka, A. Z.; Gnanakaran, S.; Triechel, M.; Hochstrasser, R. M. *J. Chem. Phys.* **1995**, *103*, 6498.
(16) Egorov, S. A.; Everitt, K. F.; Skinner, J. L. *J. Phys. Chem. A* **1999**, *103*, 9494.
(17) Egorov, S. A.; Skinner, J. L. *J. Chem. Phys.* **2000**, *112*, 275.
(18) Everitt, K. F.; Skinner, J. L. *J. Chem. Phys.* **1999**, *110*, 4467.
(19) Benjamin, I.; Whitnell, R. M. *Chem. Phys. Lett.* **1993**, *204*, 45.
(20) Johnson, A. E.; Levinger, N. E.; Barbara, P. F. *J. Phys. Chem.* **1992**, *96*, 7841.
(21) Hamm, P.; Lim, M.; Hochstrasser, R. M. *J. Chem. Phys.* **1997**, *107*, 10523.
(22) Rey, R.; Hynes, J. T. *J. Chem. Phys.* **1998**, *108*, 142.
(23) Dlott, D. D. *Chem. Phys.* **2001**, *266*, 149.
(24) Iwaki, L. K.; Dlott, D. D. *J. Phys. Chem. A* **2000**, *104*, 9101.
(25) Hamm, P.; Lim, M.; DeGrado, W. F.; Hochstrasser, R. M. *Proc. Natl. Acad. Sci. U.S.A.* **1999**, *96*, 2036.
(26) Hamm, P.; Lim, M.; Hochstrasser, R. M. *J. Phys. Chem. B* **1998**, *102*, 6123.
(27) Zanni, M. T.; Granakaran, S.; Stenger, J.; Hochstrasser, R. M. *J. Phys. Chem. B* **2001**, *105*, 6520.
(28) Zanni, M. T.; Ge, N.-H.; Kim, Y. S.; Hochstrasser, R. M. *Proc. Natl. Acad. Sci. U.S.A.* **2001**, *98*, 11265.
(29) Zanni, M. T.; Asplund, M. C.; Hochstrasser, R. M. *J. Chem. Phys.* **2001**, *114*, 4579.
(30) Ge, N. H.; Zanni, M.; Hochstrasser, R. M. *J. Phys. Chem. A* **2002**, *106*, 962.
(31) Gnanakaran, S.; Hochstrasser, R. M. *Biophys. J.* **2001**, *80*, 1254.
(32) Silbey, R. *Annu. Rev. Phys. Chem.* **1976**, *27*, 203.
(33) Woutersen, S.; Mu, Y.; Stock, G.; Hamm, P. *Proc. Natl. Acad. Sci. U.S.A.* **2001**, *98*, 11254.
(34) Gnanakaran, S.; Hochstrasser, R. M. *J. Am. Chem. Soc.* **2001**, *in press*.
(35) Lian, T.; Locke, B.; Kholodenko, Y.; Hochstrasser, R. M. *J. Phys. Chem.* **1994**, *98*, 11648.
(36) Hochstrasser, R. M. *Chem. Phys.* **2001**, *266*, 273.
(37) Madison, V.; Kopple, K. D. *J. Am. Chem. Soc.* **1980**, *102*, 4855.
(38) Krimm, S.; Bandekar, J. *Adv. Protein Chem.* **1986**, *38*, 181.
(39) Torii, H.; Tasumi, M. *J. Chem. Phys.* **1992**, *96*, 3379.
(40) Hamm, P.; Hochstrasser, R. M. In *Ultrafast Infrared and Raman Spectroscopy*; Fayer, M. D., Ed.; Marcel Dekker Inc.: New York, 2000; p 273.